

## Relationships between gas-liquid interfacial surface area, liquid saturation, and light transmission in variably saturated porous media

Michael R. Niemet,<sup>1,2</sup> Mark L. Rockhold,<sup>1,3</sup> Noam Weisbrod,<sup>1,4</sup> and John S. Selker<sup>1</sup>

Received 19 July 2001; revised 22 January 2002; accepted 22 January 2002; published 8 August 2002.

[1] Liquid saturation and gas-liquid interfacial area are important parameters for evaluating the transport and fate of contaminants in unsaturated subsurface environments. Recent findings indicate that interfacial surface area controls the relative degree of transmitted light in laboratory systems containing translucent porous media. Equations are derived to estimate the specific gas-liquid interfacial area from the area under the primary-drainage branch of the  $S_{\text{eff}}-h$  characteristic curve as parameterized using common water retention functions. The total area under the curve provides the maximum available specific gas-liquid interfacial area available at residual saturation, which can be incorporated into the relationship to determine the gas-liquid interfacial area at intermediate degrees of saturation via light transmission. Experimental results, and analysis of external data sets, support these findings. Closed-form relationships are presented as enhancements to a recent method for determination of liquid saturations above residual using light transmission. A physically based model is developed and tested for the quantification of liquid contents below residual saturation. *INDEX TERMS:* 1829 Hydrology: Groundwater hydrology; 1866 Hydrology: Soil moisture; 1875 Hydrology: Unsaturated zone; 1894 Hydrology: Instruments and techniques; *KEYWORDS:* light transmission, gas-liquid interfacial surface area, liquid saturation, residual saturation, unsaturated porous media, characteristic curve

### 1. Introduction

[2] With the advent of modern digital cameras and powerful inexpensive computing resources, quantitative digital imaging methods have permeated virtually all fields of science and engineering. In the area of nondestructive, noninvasive laboratory measurement of liquid saturation in translucent porous media, methods utilizing the degree of transmitted light have gained considerable appeal [e.g., Niemet and Selker, 2001; Darnault et al., 2001, 1998; Mortensen et al., 2001; Kechavarzi et al., 2000; DiCarlo et al., 1999; Weisbrod et al., 2002]. Until recently, the use of light transmission has been less desirable, in most instances, to more traditional electromagnetic measurement methods such as gamma ray [Oostrom et al., 1998; Gardner, 1986] and X-ray attenuation [Rimmer et al., 1998; Tidwell and Glass, 1994; Liu et al., 1993]. The reasons for this are primarily threefold: (1) physical/optical limitations, (2) difficulties in gravimetric calibration of the system, and (3) the lack of robust physical models, free of empirical fitting parameters, which accurately predict the degree of liquid saturation from the degree of transmitted light.

[3] Because of the relatively low energy of visible light, much thinner sample sections are required for light trans-

mission systems than for gamma ray and X-ray systems. Also, the media must be sufficiently translucent to allow a readily quantifiable fraction of the source light to transmit through the sample. The planar containment boundary in two-dimensional (2-D) systems results in the particle packing adjacent to the containment sheets being less dense than within the body matrix. This could potentially result in the short-circuiting of flow through the pores adjacent to the boundary walls under saturated conditions. However, under unsaturated conditions, flow would tend to occur primarily in the smaller pores, away from the walls. In excessively thin 2-D sample sections, the ability to obtain a maximum packing density between containment sheets may be hindered, effectively altering the properties of the porous media throughout. Given these considerations, it is important to ensure that the average porosity with a 2-D light transmission system is similar to that observed in 3-D packs of the same material.

[4] To correlate light transmission to measured gravimetric values of liquid saturation requires gravimetric measurements of the order of a millimeter to capture the rapidly changing character of most sands between residual and complete saturation. Also, undisturbed samples are difficult to obtain from within the light transmission chambers. The primary factor holding back the development of physical models relating light transmission to liquid saturation is that light attenuation through the porous media is not entirely controlled by absorption through the liquid, solid, and gaseous phases within the porous media (Beer's law absorption), as is the case with the higher-energy electromagnetic methods. Light is also lost at the interfaces between phases (Fresnel losses).

[5] Recently, a physical model was developed based on the premise that the degree of light transmission, relative to

<sup>1</sup>Department of Bioengineering, Oregon State University, Corvallis, Oregon, USA.

<sup>2</sup>Now at CH2M Hill, Corvallis, Oregon, USA.

<sup>3</sup>Now at Pacific Northwest National Laboratory, Richland, Washington, USA.

<sup>4</sup>Now at Department of Environmental Hydrology and Microbiology, Ben-Gurion University of the Negev, Sde-Boqer, Israel.

saturated conditions, is controlled by the fraction of available gas-liquid interfacial area exposed within the measurement volume [Niemet and Selker, 2001]. The assumption of uniform-sized pores was avoided since the pore size distribution of a particular media is implicitly contained within the characteristic curve of relative light transmission versus capillary pressure head, between residual and complete saturation. All of the parameters needed to completely characterize this model for a particular media were obtained from this single characteristic curve. The accuracy of this model, and the system employed, was conservatively estimated to be within  $\pm 2.3\%$  saturation over the entire domain under both drainage and infiltration experiments.

[6] The method described above requires the numerical integration of the discrete data points which comprise the relative light transmission versus capillary pressure head curve, between residual and complete saturation. This result is then fit with a fourth-order polynomial in order to relate saturation to any degree of light transmission, provided the liquid saturation is above residual. An alternative approach would be to fit the discrete light transmission versus capillary pressure head data with a continuous function at the outset, and then the function can be integrated analytically to obtain a closed-form solution between light transmission and liquid saturation. Consideration of liquid contents between residual and complete saturation is sufficient for most experimental needs. However, certain situations require the determination of saturations below residual, such as in experiments involving vapor transport from residually saturated media [Kelly and Selker, 2001; Weisbrod et al., 2000].

[7] In this paper our primary objectives are (1) to further explore the relationship between gas-liquid surface area and light transmission, and examine the potential of light transmission as an analytical tool to measure the gas liquid interfacial area in unsaturated porous media; (2) to develop and test a physical model to predict liquid saturation from light transmission for saturations below residual; and (3) to present closed-form solutions relating liquid saturation to light transmission based on the widely used Brooks and Corey [1964] and van Genuchten [1980] water retention functions.

## 2. Gas-Liquid Interfacial Area

[8] The gas-liquid interface plays a crucial role in the transport of nonaqueous phase liquids (NAPLs), colloids, bacteria, and other contaminants in unsaturated porous media since these components often tend to adsorb to interfacial surfaces [Bradford and Leij, 1997; Schäfer et al., 1998]. In two-fluid systems (e.g., solid, liquid, and gas phases), the maximum degree of gas-liquid interfacial area available for a particular porous medium occurs at, or near, residual liquid saturation. Standard analytical methods are available for measuring the surface area of a porous medium based on molecular adsorption and the resulting physical and chemical responses [Carter et al., 1986]. However, these measurements include the surface area of internal micropores and other small defects in the particle grains and can yield surface areas that may be much larger than those pertinent to fluid flow and contaminant transport [Bradford and Leij, 1997]. In the following discussion it is assumed that microporosity does not contribute to the

effective surface area of the particles when continuous liquid films are ubiquitous. This is taken to be the case at residual liquid saturation, where the gas-liquid surface area approaches the surface area of the particles and the liquid film covers the particles in a uniform, very thin film.

[9] Geometrically based relationships have been presented to estimate the total surface area for any packing of spheres [Gvirtzman and Roberts, 1991; Bear, 1972]. The particle surface area per unit bulk volume of packed spheres,  $M$ , is given by [Bear, 1972, page 51]

$$M = \frac{A_T}{V_B} = \frac{3(1 - \phi)}{\bar{r}}, \quad (1)$$

where  $A_T/V_B$  is the total interstitial surface area per unit bulk volume of the pore space,  $\bar{r}$  is the harmonic mean radius of the spheres, and  $\phi$  is the porosity. It follows, then, that for porous media whose harmonic mean radius approaches its arithmetic mean,

$$\frac{A_T}{V_B} = \frac{6(1 - \phi)}{d_{50}}, \quad (2)$$

where  $d_{50}$  is the mass-based mean particle diameter. Note that since these equations assume smooth spherical particles, the total specific surface area is representative both of the surface area of the particles under dry conditions and the air-water interfacial area under residually saturated conditions, if the liquid film is assumed to be negligibly thin.

[10] Cary [1994, equation (4)] noted that the total specific air-water surface area of a porous medium could be determined from the water retention relation based on the capillary tube analogy. Expressed in the notation used here, the relationship is

$$\frac{A}{V_B} = \frac{\rho g \phi}{\sigma} \sum_{S_{\text{eff}}=1}^{S_{\text{eff}}} h \Delta S_{\text{eff}}, \quad (3)$$

where  $\rho$  is the density of the liquid (water),  $\sigma$  is the surface tension of the liquid,  $g$  is the gravitational constant, and  $S_{\text{eff}}$  is the effective liquid saturation.

[11] For liquid saturations above residual, various other models for predicting gas-liquid interfacial area have been presented based upon the areas of concave interfaces [Frankenfield and Selker, 1994; Gvirtzman and Roberts, 1991; Skopp, 1985], a pore-scale network model [Reeves and Celia, 1996], and thermodynamics [Bradford and Leij, 1997; Miller et al., 1990; Leverett, 1941]. Surfactant adsorption has also been used for laboratory measurement of gas-liquid interfacial area in porous media [Shaefer et al., 2000; Saripalli et al., 1997; Kim et al., 1997; Karkare and Fort, 1996].

[12] Niemet and Selker [2001] suggested that the relationship between the exposed fraction of gas-liquid interfacial area  $A/A_T$  to the relative degree of light transmission through porous media was given by

$$\frac{A}{A_T} = \frac{\ln\left(\frac{I}{I_s}\right)}{\ln\left(\frac{I_{\text{res}}}{I_s}\right)}, \quad (4)$$

where  $I$  is the intensity of transmitted light under the condition of interest.  $I_s$  and  $I_{\text{res}}$  are the transmitted

intensities under saturated and residual liquid saturation, respectively. A nearly linear correspondence was observed between the log-scaled relative degree of light transmission and water saturation, suggesting a linear relationship between air-water interfacial area and saturation as well, as indicated by equation (4). This was supported by the observations of *Schaefer et al.* [2000] and *Kim et al.* [1997], which showed a nearly linear relationship between air-water interfacial area and saturation following drainage from fully saturated conditions.

[13] Another approach to determine the gas-liquid interfacial area can be derived from a distribution of spherical pores. The assumption of spherical pores may be geometrically simplistic; however, it maintains that the pores are discrete and symmetrical in all three dimensions, while being readily applicable to the classical drainage relationship for porous media. Provided the media is draining from saturation, the Laplace equation (contact angle = 0°) defines the pore radius  $r$  that will drain at a specific pressure head  $h$

$$h = \frac{2\sigma}{\rho g r}. \quad (5)$$

Given the volume and surface area of a sphere are  $(4\pi r^3)/3$  and  $4\pi r^2$ , respectively, the volume to surface area relationship for a single spherical pore that will drain at pressure head  $h$  is

$$V_r = \frac{2\sigma}{3\rho g} \frac{A_r}{h}, \quad (6)$$

where  $A_r$  and  $V_r$  are the effective surface area and volume of the pore. Equation (6) is a factor of 1/4 less than a similar equation presented by *Niemet and Selker* [2001, equation (17)]. The difference is a result of being based on the cross-sectional area of a sphere rather than the surface area, which differ by a factor of 4.

[14] During drainage the pores drain sequentially from largest to the smallest. Equation (6) can be rewritten as a differential to express the incremental contribution of a single pore within a continuous range of pores as

$$dV_p = \frac{2\sigma}{3\rho g} \frac{dA_p}{h}, \quad (7)$$

where  $V_p$  and  $A_p$  represent the total effective drained pore volume and surface area, respectively, within the range of pore sizes considered. The incremental drained volume,  $dV_p$ , is related to the incremental change in effective saturation  $S_{\text{eff}}$  as follows:

$$dV_p = \phi V_B d(1 - S_{\text{eff}}). \quad (8)$$

Combining equations (7) and (8) and solving for  $dA_p$  yields

$$dA_p = \frac{3\rho g \phi}{2\sigma} V_B h d(1 - S_{\text{eff}}). \quad (9)$$

The specific gas-liquid surface area  $A/V_B$  can be determined by integrating equation (9) as follows:

$$\frac{A}{V_B} = \frac{3\rho g \phi}{2\sigma} \int_{1-S_{\text{eff}}=0}^{1-S_{\text{eff}}} h d(1 - S_{\text{eff}}) = \frac{3\rho g \phi}{2\sigma} \int_{S_{\text{eff}}=1}^{S_{\text{eff}}} h dS_{\text{eff}}. \quad (10)$$

[15] Note that equation (10) is 1.5 times greater than the results of *Cary* [1994], presented here as equation (3), which was derived under the capillary tube analogy. Geometrically, this is to be expected since the specific volume of a sphere is a factor of 1.5 greater than that of a cylinder of the same radius. The total specific gas-liquid interfacial area,  $A_T/V_B$ , can be found by integrating equation (10) from complete to residual saturation. The integral in equation (10) represents the area under the  $S_{\text{eff}}-h$  characteristic curve. Therefore equation (10) indicates that the specific surface area is proportional to the area under the effective saturation characteristic curve, integrated from  $S_{\text{eff}} = 1$  toward the dry end, provided the media is drained from saturation. It is important to observe that since equation (10) is expressed in terms of the primary drainage curve, it is not capable of handling the effects of rewetting; however, the total gas-liquid surface area at residual saturation is largely determined by the specific surface area of the particles and thus is not affected by hysteresis. The proportionality of the air-water interfacial area to the area under the characteristic curve was observed experimentally by *Bradford and Leij* [1997].

[16] The specific surface area can be computed numerically given a set of discrete  $S_{\text{eff}}$  versus  $h$  data points, or determined analytically from solution of a continuous function that characterizes a particular media (e.g., *Brooks and Corey* [1964] or *van Genuchten* [1980]). The typical  $S_{\text{eff}}-h$  form of the Brooks and Corey equation is

$$S_{\text{eff}} = \left(\frac{h_d}{h}\right)^\lambda, \quad (11)$$

where  $\lambda$  is an empirical fitting parameter that is optimized along with the air-entry pressure head  $h_d$  such that a best fit is obtained to the data. For  $h < h_d$ ,  $(h_d/h) = 1$ . Substitution of equation (11) into (10) and integrating with respect to  $S_{\text{eff}}$  yields

$$\frac{A}{V_B} = \frac{3\rho g \phi}{2\sigma} \frac{h_d}{\left(1 - \frac{1}{\lambda}\right)} \left(1 - S_{\text{eff}}^{1-\frac{1}{\lambda}}\right). \quad (12)$$

Similarly, for a van Genuchten type function of the form

$$S_{\text{eff}} = \left(\frac{1}{1 + (\alpha h)^n}\right)^m, \quad (13)$$

where  $\alpha$ ,  $m$ , and  $n$  are empirical fitting parameters, solving equation (13) for  $h$ , substituting into (10), and integrating with respect to  $S_{\text{eff}}$  yields

$$\frac{A}{V_B} = \frac{3\rho g \phi}{2\sigma} \frac{1}{\alpha} \int_{S_{\text{eff}}=1}^{S_{\text{eff}}} \left(S_{\text{eff}}^{-\frac{1}{m}} - 1\right)^{\frac{1}{n}} dS_{\text{eff}}. \quad (14)$$

Using the substitutions  $u = S_{\text{eff}}^{1/m}$ ,  $w = m - (1/n)$ , and  $z = 1 + (1/n)$  yields

$$\begin{aligned} \frac{A}{V_B} &= \frac{3\rho g\phi}{2\sigma} \frac{m}{\alpha} \int_1^u u^{w-1} (1-u)^{z-1} du \\ &= \frac{3\rho g\phi}{2\sigma} \frac{m}{\alpha} \left[ \int_0^1 u^{w-1} (1-u)^{z-1} du - \int_0^u u^{w-1} (1-u)^{z-1} du \right] \end{aligned} \quad (15)$$

where  $0 \leq u \leq 1$ . From standard identities, equation (15) can be expressed as

$$\frac{A}{V_B} = \frac{3\rho g\phi}{2\sigma} \frac{m}{\alpha} B(w, z) [1 - I_u(w, z)], \quad (16)$$

where  $B(w, z)$  represents the beta function of  $w$  and  $z$  and  $I_u(w, z)$  is the incomplete beta function of  $w$  and  $z$  [Abramowitz and Stegun, 1965, pp. 258 and 944].

### 3. Liquid Saturation

[17] As noted in equation (4), the exposed fraction of gas-liquid interfacial area dictates the relative degree of light transmission through porous media. Given this relationship, and certain assumptions, closed-form solutions can be derived relating the degree of liquid saturation to light transmission through unsaturated translucent porous media. However, separate relationships are required for conditions above and below residual saturation.

#### 3.1. Saturation Above Residual

[18] The effective degree of saturation is related to light transmission as described by Niemet and Selker [2001] for saturations above residual

$$S_{\text{eff}} = 1 - \left( \int_0^\Omega \frac{d\Omega}{h} \right) / \left( \int_0^1 \frac{d\Omega}{h} \right), \quad (17)$$

where

$$\Omega = \ln \left( \frac{I}{I_s} \right) / \ln \left( \frac{I_{\text{res}}}{I_s} \right). \quad (18)$$

$\Omega$  then represents the log-scaled relative degree of light transmission. Numerical integration of the  $\Omega$ - $h$  data set in equation (17) results in a set of discrete points relating light transmission to effective saturation. These data can then be fit by a fourth-degree polynomial to obtain a continuous  $S_{\text{eff}}$ - $\Omega$  relationship, such that

$$S_{\text{eff}} = a\Omega^4 - b\Omega^3 + c\Omega^2 - d\Omega + 1, \quad (19)$$

where  $a$ ,  $b$ ,  $c$ , and  $d$  are empirically determined coefficients. The absolute saturation  $S$  can be determined as follows:

$$S = S_{\text{eff}}(1 - S_{\text{res}}) + S_{\text{res}}. \quad (20)$$

[19] An alternative approach, presented here, is to fit the  $\Omega$ - $h$  curve with a continuous function, then solve equation

(17) analytically for the  $S$ - $\Omega$  relationship. The  $\Omega$ - $h$  curve is similar in shape to a typical  $S$ - $h$  characteristic curve and is therefore amenable to fitting by equations of the same form as the widely used water retention functions defined by Brooks and Corey [1964] and van Genuchten [1980].

[20] The Brooks and Corey model can be applied to the  $\Omega$ - $h$  curve as follows:

$$1 - \Omega = \left( \frac{h_d}{h} \right)^\lambda, \quad (21)$$

where for  $h < h_d$ ,  $(h_d/h) = 1$ . The prime was added to  $\lambda$  to avoid confusion with the similar parameter fit to the  $S_{\text{eff}}$ - $h$  curve in equation (11); however,  $h_d$  is the same for both equations. Solving for  $1/h$  yields

$$\frac{1}{h} = \frac{(1 - \Omega)^{\frac{1}{\lambda}}}{h_d}. \quad (22)$$

Integrating both sides with respect to  $\Omega$  and substitution into equation (17) yields

$$S_{\text{eff}} = (1 - \Omega)^{\frac{1}{\lambda} + 1}. \quad (23)$$

$S$  can then be determined from  $S_{\text{eff}}$  by means of equation (20) using only one fitting parameter instead of four.

[21] The van Genuchten model can be applied to the  $\Omega$ - $h$  curve as follows

$$1 - \Omega = \left( \frac{1}{1 + (\alpha h)^{n'}} \right)^{m'}. \quad (24)$$

Again, the prime notation is used to avoid confusion with parameters unique to the  $S_{\text{eff}}$ - $h$  equations. Solving for  $1/h$  yields

$$\frac{1}{h} = \alpha \left[ (1 - \Omega)^{-\frac{1}{m'}} - 1 \right]^{-\frac{1}{n'}}, \quad (25)$$

and taking the integral of both sides with respect to  $\Omega$  results in

$$\int \frac{d\Omega}{h} = \alpha \int \left[ (1 - \Omega)^{-\frac{1}{m'}} - 1 \right]^{-\frac{1}{n'}} d\Omega. \quad (26)$$

Using the substitutions  $u' = (1 - \Omega)^{1/m'}$ ,  $w' = m' + (1/n')$  and,  $z' = 1 - (1/n')$ , yields

$$\begin{aligned} \int \frac{du'}{h} &= -\alpha m' (-1)^{m'-1} \int u'^{m'-1+\frac{1}{n'}} (1-u')^{-\frac{1}{n'}} du' \\ &= -\alpha m' (-1)^{m'-1} \int u'^{w'-1} (1-u')^{z'-1} du' \end{aligned} \quad (27)$$

Equation (17) can now be represented in terms of  $u'$  as

$$S_{\text{eff}} = 1 - \frac{\int_0^1 \frac{du'}{h} - \int_0^{u'} \frac{du'}{h}}{\int_0^1 \frac{du'}{h}} = \frac{\int_0^{u'} u'^{w'-1} (1-u')^{z'-1} du'}{\int_0^1 u'^{w'-1} (1-u')^{z'-1} du'}, \quad (28)$$



where  $0 \leq u' \leq 1$ . The denominator of equation (28) represents the beta function of  $w'$  and  $z'$ ,  $B(w', z')$ , and the numerator is the product of the incomplete beta function and the beta function,  $I_u(w', z')B(w', z')$ . Thus

$$S_{\text{eff}} = \frac{I_u(w', z')B(w', z')}{B(w', z')} = I_u(w', z'). \quad (29)$$

$S$  can be determined from  $S_{\text{eff}}$  by means of equation (20).

### 3.2. Saturation Below Residual

[22] Consider a porous medium to be represented by pores of various sizes and that at residual saturation, all pores are drained but the solid surfaces remain coated by a thin, continuous film of liquid. Once the media dries past this point, a solid-gas interface is created where there were previously liquid-gas and solid-liquid interfaces. By incorporating the absorptive and interfacial losses, the degree of transmitted light relative to a source intensity,  $I_0$ , through completely dry, completely saturated, and residually saturated porous medium ( $I_d$ ,  $I_s$ , and  $I_{\text{res}}$ ) are [Niemet and Selker, 2001]:

$$I_d = I_0 \tau_{pg}^{2k} \exp(-\alpha_p d_p k) \quad (30)$$

$$I_s = I_0 \tau_{pl}^{2k} \exp(-\alpha_p d_p k) \quad (31)$$

$$I_{\text{res}} = I_0 \tau_{pl}^{2k} \tau_{lg}^{2k} \exp(-\alpha_p d_p k), \quad (32)$$

respectively, where  $\alpha_p$  is the absorption coefficient of the solid particles;  $d_p$  is the average diameter of the pores;  $k$  is the number of pores across the media thickness;  $\tau_{pl}$  is the transmittance of the solid-liquid interface;  $\tau_{pg}$  is the transmittance of the solid-gas interface; and  $\tau_{lg}$  is the transmittance of the liquid-gas interface.

[23] Defining  $\hat{S}_{\text{eff}}$  as the effective degree of saturation between residual saturation and air-dry conditions (i.e.,  $\hat{S}_{\text{eff}} = 1$  when  $S = S_{\text{res}}$  and  $\hat{S}_{\text{eff}} = 0$  when  $S = 0$ ), then if the film thickness is considered to be constant throughout the media,  $\hat{S}_{\text{eff}}$  represents the extent of film coverage. A general light transmission equation for liquid saturations between dry and residual extremes, which accounts for losses at all possible interfaces, can be expressed by

$$I = I_0 \tau_{pg}^{2k(1-\hat{S}_{\text{eff}})} \tau_{pl}^{2k\hat{S}_{\text{eff}}} \tau_{lg}^{2k\hat{S}_{\text{eff}}} \exp(-\alpha_p d_p k). \quad (33)$$

Note that equations (30) through (32) are special cases of (33). Dividing equation (33) by (30) results in

$$\frac{I}{I_d} = \tau_{pg}^{-2k\hat{S}_{\text{eff}}} \tau_{pl}^{2k\hat{S}_{\text{eff}}} \tau_{lg}^{2k\hat{S}_{\text{eff}}}, \quad (34)$$

and solving for  $\hat{S}_{\text{eff}}$  yields

$$\hat{S}_{\text{eff}} = \frac{\ln\left(\frac{I}{I_d}\right)}{\ln\left(\frac{I_{\text{res}}}{I_d}\right)} = \frac{\ln\left(\frac{I_s}{I_d} \frac{I}{I_s}\right)}{\ln\left(\frac{I_{\text{res}}}{I_d} \frac{I_{\text{res}}}{I_s}\right)}. \quad (35)$$

The latter form of equation (35) is expressed relative to completely saturated conditions. However, the initial form

of the equation can be used in the absence of the saturated data. Values of  $I_s/I_d$  and  $I_{\text{res}}/I_s$  are not obtained on a pixel-by-pixel basis, but instead represent average values for a given media packing. If the initial form of the equation is desired,  $I_{\text{res}}/I_d$  can be determined as described later. The absolute saturation below residual can then be determined by

$$S = S_{\text{res}} \hat{S}_{\text{eff}}. \quad (36)$$

[24] The error associated with light transmission measurements of liquid saturation above residual saturation was reported to be within 2.3%. The error, stated in this way, suggests that a similar technique may not be applicable to liquid saturations below residual, which is generally less than 6%. However, the reported error value represented an overall systematic error, by comparing the accuracy of the sum of all measurements within the domain to a known overall volumetric change in water. This error value in no way suggests that the system is not able to quantifying changes in saturation below 2.3%. The dynamic range of a typical 14-bit digital charge-coupled-device (CCD) camera is capable of statistically quantifying changes in light intensity of less than one part in 16,000. However, the accuracy of a measurement at a single pixel is subject to many different noise elements. Weisbrod *et al.* [2002] determined the pixel-to-pixel saturation variability ( $\pm 3$  standard deviations) in a similar system to be about 2%. When looking at the volumetric change in water over a large region of pixels the random noise is eliminated in the summation process.

## 4. Materials and Methods

[25] A 2-D light transmission system similar to that of Niemet and Selker [2001] was used in all experiments and consisted primarily of a chamber, light source, and detector. A front view of the light transmission chamber is shown in Figure 1, whose sand-packed region dimensions were 1 cm thick  $\times$  45.5 cm wide  $\times$  45.5 cm high. The laboratory environment which contained the system was thermostatically maintained at  $21.5 \pm 1.0^\circ\text{C}$ . A thermoelectrically cooled, 14-bit, gray scale,  $768 \times 512$  pixel, CCD camera (ISI Systems, Santa Barbara, California) was used to quantify light transmission, except for the drying below residual experiment, where a liquid-cooled, 16-bit, gray scale,  $512 \times 512$  pixel CCD (Princeton Instruments, Trenton, New Jersey) was used. A 620-nm center-wavelength, 10-nm band-pass, filter (Oriel, Stratford, Connecticut) was employed to limit the chromatic range of quantification. Aperture settings ranged from F4 to F8, and exposure times varied from 0.5 to 1.8 s depending on the camera and sand grade. Each pixel on an image represented  $1 \text{ mm}^2$  of porous media for both systems.

[26] The porous media used was Accusand (Unimin, Le Sueur, Minnesota) silica sands in 12/20, 20/30, 30/40, and 40/50 grades. The average particle diameters ( $d_{50}$ ) for these sands are 1.105, 0.713, 0.532, and 0.359 mm, respectively. Major physical properties of the sands are summarized by Schroth *et al.* [1996]. Preparations for all experiments consisted of dry packing the chamber with sand and subsequent saturation with distilled water. For each packing, preexperimental light transmission images were obtained

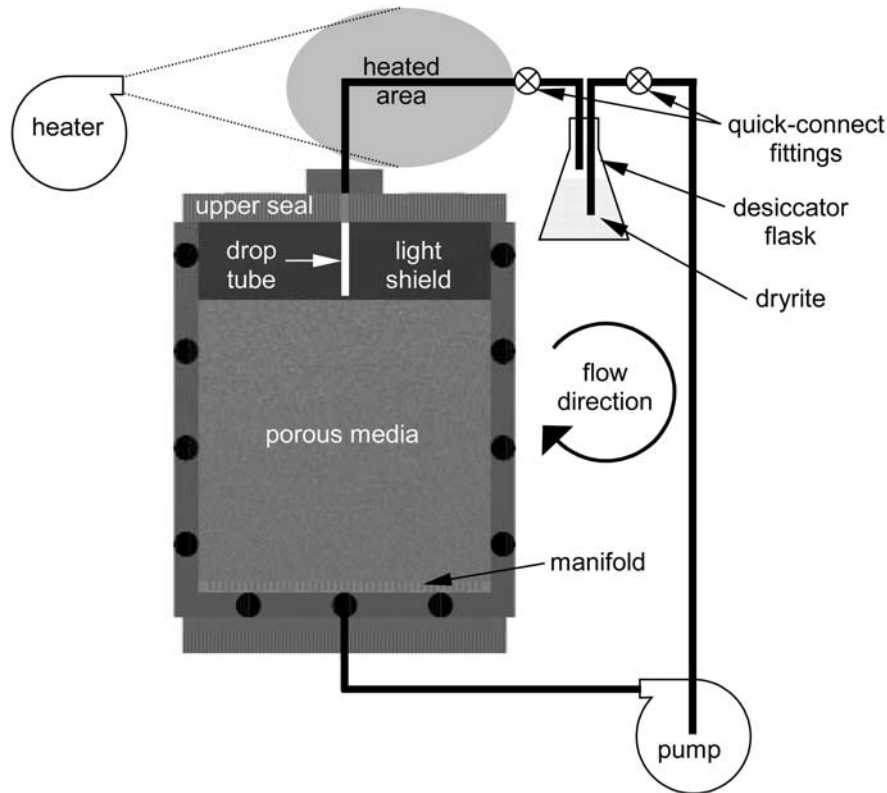


**Figure 1.** Schematic of the experimental system where saturation below residual was studied.

under dry and saturated conditions. Bias and dark signal contributions were removed from all raw data images prior to the saturation calculations by subtracting an image of equal exposure time obtained with the source lighting off. Water saturation was determined for each point on an image (pixel) within the media-filled region by either equation (20) or (36), depending on whether the relative degree of light transmission was greater than or less than the average value of  $I_{res}/I_s$  for that pack (Table 1).

[27] A set of experiments was performed to obtain the light transmission versus pressure head curves for each of the four sand grades. These were carried out by first slowly removing water from the saturated chamber's lower drainage port with a low-flow valveless piston pump (Fluid-Metering, model RH0CKC). The rate was such that the zero-pressure level, measured with a piezometer, was at the chamber's lower boundary after 48 hours (between 5 and 11 mL/h, depending on sand grade). Since the drainage rate was very slow and uniform, the systems were assumed to represent hydrostatic, primary drainage conditions. Images were taken of these variably saturated systems, which

ranged from residual saturation at the upper boundaries to completely saturated near the lower boundaries.

[28] To test the ability of equation (36) to accurately predict water saturations below residual, a drying experiment was performed with 40/50 sand. In this case, following saturation the chamber was drained over the course of an hour with a peristaltic pump. Subsequently, the pumping rate was increased about fivefold to remove most of the water that remained in the capillary fringe at the bottom of the chamber, within the plenum beneath the lower manifold screen, and in the tubing. At this point, the chamber was entirely unsaturated with a portion remaining above residual saturation near the lower manifold boundary. An image was obtained of this condition. Next, a closed recirculating system was established with a desiccating flask filled with Dryrite (Hammond, Xenia, Ohio) as shown in Figure 1. The drying process was initiated by pumping gas in the clockwise direction at about 1.2 L/min such that vapor-laden air from the pore space was dried in the desiccator and then recycled back into the chamber through the lower port. The mass of water removed from the chamber was monitored by

**Table 1.** Selected Properties of the Accusands From Niemet and Selker [2001]

Sand	$I_d/I_s^a$	$I_{res}/I_s^a$	$S_{res}^b$	$a^a$	$b^a$	$c^a$	$d^a$	$d_{50}^b$ , mm	Porosity
12/20	0.134	0.258	0.034	0.87	1.45	1.00	1.42	1.105	0.335
20/30	0.085	0.200	0.046	0.57	0.94	0.64	1.27	0.713	0.333
30/40	0.041	0.135	0.052	0.26	0.39	0.29	1.16	0.532	0.327
40/50	0.016	0.070	0.057	0.19	0.24	0.19	1.14	0.359	0.332

<sup>a</sup>These parameters are strongly wavelength dependent and apply only to data obtained using a 620-nm center wavelength, 10-nm band-pass filter.

<sup>b</sup>From Schroth et al. [1996].

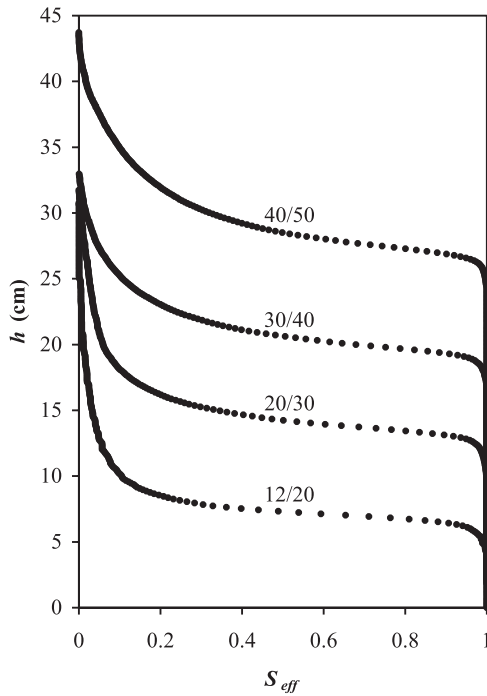


**Figure 2.** Capillary pressure head versus effective saturation for the four grades of Accusand.

periodically weighing the desiccating flask until the media was dry. Images were obtained simultaneously with the mass measurements. The pump and source lighting were shut down overnight and restarted on subsequent days.

[29] The total volume of resident water  $V$  in the chamber for each image was computed by summing over all pixels

$$V = \sum S V_{\text{pix}} \phi, \quad (37)$$

where,  $V_{\text{pix}}$  is the bulk volume of chamber space occupied by a pixel and  $\phi$  is the porosity of the packing. The predicted water removed from the chamber at any point in time ( $\Delta V$ ) was computed by the difference between the predicted volume for the image prior to the initiation of drying ( $V_0$ ) and the predicted volume for the image of interest ( $V_i$ )

$$\Delta V = V_0 - V_i. \quad (38)$$

## 5. Results and Discussion

### 5.1. Gas-Liquid Interfacial Surface Area

[30] The  $S_{\text{eff}}-h$  characteristic curves for the four sands are shown in Figure 2 and were obtained through numerical

integration of the  $\Omega-h$  data in equation (17) by the trapezoid rule. The total areas under these curves are summarized in Table 2. The total specific air-water interfacial surface areas,  $A_T/V_B$ , for the four grades of Accusand are also shown in Table 2, computed using equations (2) and (10). The density and surface tension of the distilled water employed were measured to be  $0.993 \text{ g/cm}^3$  and  $72.8 \text{ dynes/cm}$  [Weisbrod *et al.*, 2002].

[31] The values computed from equation (10) were 1.5 (12/20), 1.8 (20/30), 1.9 (30/40), and 1.8 (40/50) times those computed by equation (2). Note that the capillary tube based equation (3) predicts exactly 1.5 times less total specific surface area than equation (10), which is within the range of values predicted by equation (2). For the given mean grain diameters, the specific surface areas determined by equation (2) fall within the range presented by Gvirtzman and Roberts [1991] for cubic and rhombohedral packs of identical spheres. Schaefer *et al.* [2000] measured a total air-water interfacial area at residual saturation for 40/50 Accusand of about  $200 \text{ cm}^2/\text{cm}^3$  using an anionic surfactant method [Saripalli *et al.*, 1997], which is only 1.5% above the value of  $197 \text{ cm}^2/\text{cm}^3$  computed using equation (10) for the 40/50 sand used here.

[32] The average area under the primary drainage characteristic curves of Schaefer *et al.* [2000] was about a factor of 3 less than observed here. The two sodium dodecyl benzene sulfonate (SDBS) solutions employed by Schaefer *et al.* [2000] had surface tensions of 44 and 28 dynes/cm, whose lower surface tension (36, on average, versus 72.8 dynes/cm for pure water) along with a higher porosity (42 versus 33% here) explain the lower capillary rise. The average area under the curve, surface tension, and porosity from Schaefer *et al.* [2000] yield a specific surface area of about  $170 \text{ cm}^2/\text{cm}^3$  via equation (10). This represents  $110 \text{ cm}^2/\text{g}$  of dry sand, calculated as follows:

$$\frac{A_T}{m_S} = \frac{A_T}{V_B} \frac{1}{\rho_S (1 - \phi)}, \quad (39)$$

where  $m_S$  is the mass of sand and  $\rho_S$  is the particle density ( $2.663 \text{ g/cm}^3$  for 40/50 Accusand [Schroth *et al.*, 1996]). Calculated in this way, the total specific surface area is independent of porosity. For the 40/50 data presented here, the total specific surface area of  $197 \text{ cm}^2/\text{cm}^3$  corresponds to  $112 \text{ cm}^2/\text{g}$  of dry sand, which is 1.8% above the value determined by Schaefer *et al.* [2000]. The similarity of the total surface area per gram of sand between these two independent experiments is supportive of the ability of equation (10) to accurately predict total gas-liquid surface area.

[33] Although the Accusand particles have a sphericity of 0.9 [Schroth *et al.*, 1996], microscopically their surfaces are

**Table 2.** Comparison of Predicted Specific Surface Areas Computed by and Equations (2) and (10)

Sand	Area Under $S_{\text{eff}}-h$ Curve (cm), Figure 2	Equation (2), $A_T/V_B$ , $\text{cm}^2/\text{cm}^3$	Equation (10), $A_T/V_B$ , $\text{cm}^2/\text{cm}^3$	Ratio
12/20	8.0	36.1	53.2	1.5
20/30	15.2	56.1	100.4	1.8
30/40	21.5	75.9	142.5	1.9
40/50	29.8	111.6	197.1	1.8

rough and irregular. These imperfections are not accounted for in the models based on perfect spheres (i.e., equation (2) and the data presented by *Gvirtzman and Roberts* [1991]), which may help to explain why these models underpredicted the total specific particle surface area by about 60% relative to equation (10) and that measured by *Schaefer et al.* [2000]. Of course, the particle surface area including internal micropores is much larger; however, this surface area is isolated and is likely not of concern for processes influenced by the gas-liquid interface.

[34] The log-scaled degrees of light transmission appear to be linearly related to the inverse of the mean grain diameter for both the  $\ln(I_{res}/I_s)$  and the  $\ln(I_d/I_s)$  as shown in Figure 3. This is to be expected if the interfacial surface area, either air-water or air-solid, is controlling the relative degree of light transmission, since these grades of Accusand have been shown to be geometrically similar [*Schroth et al.*, 1996]. Equation (2) indicates that  $A_T$  is proportional to  $1/d_{50}$ , which is not supported by the data in Figure 3 since the linear extrapolations do not pass through the origin. Examination of (10) reveals that  $A_T$  is proportional to  $1/d_{50}$  only when the resulting pore sizes are symmetrically distributed on a volumetric basis; that is, the pores above and below the mean pore size have equal capacity. This determination can be made by inference between capillary head and pore size through the Laplace equation for primary drainage (equation (5)), and recognizing that the mean pore size is proportional to the mean particle size. From Figure 2 it is apparent that the pore sizes of the four Accusands are not symmetrically distributed, further supporting the applicability of equation (10) over (2) in these sands.

[35] It is interesting to note that the ratio of the  $\ln(I_{res}/I_s)$  to the  $\ln(I_d/I_s)$  is nearly constant for all sands, as shown in

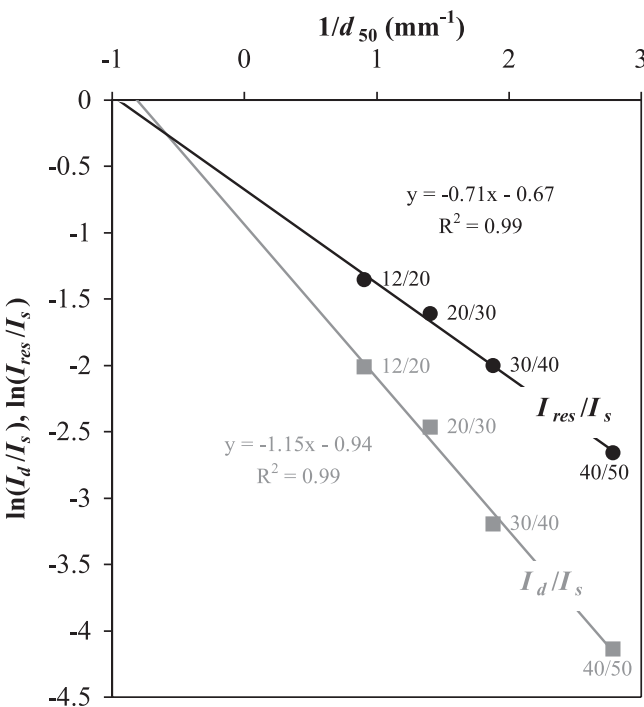


**Figure 3.** Relationship between the  $\ln(I_{res}/I_s)$  and  $\ln(I_d/I_s)$  versus  $1/d_{50}$  for the four grades of Accusand.

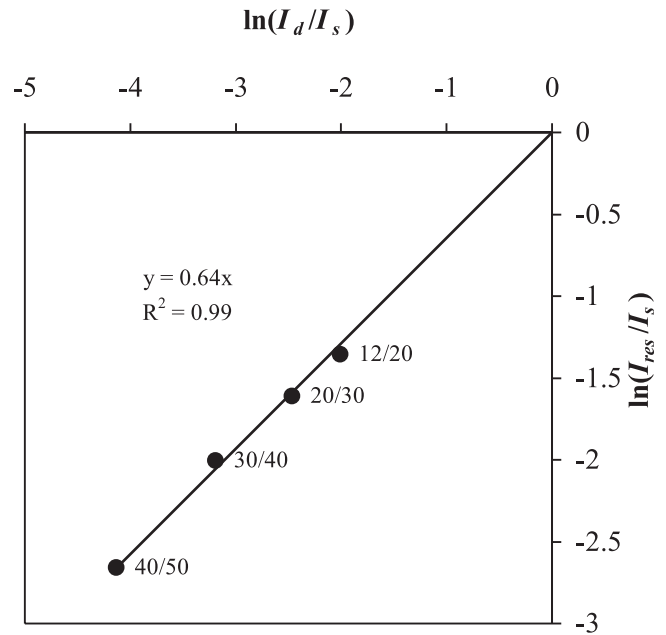


**Figure 4.** Relationship between the  $\ln(I_{res}/I_s)$  and  $\ln(I_d/I_s)$  for the four grades of Accusand.

Figure 4. It can be shown by combining equations (30) through (32) that this is not a coincidence,

$$\frac{\ln\left(\frac{I_{res}}{I_s}\right)}{\ln\left(\frac{I_d}{I_s}\right)} = \frac{\ln(\tau_{pl})}{\ln\left(\frac{\tau_{pg}}{\tau_{lg}}\right)} = C_\tau. \quad (40)$$

The constant  $C_\tau$  is determined by the relative transmittances of the solid, liquid, and gas interfaces, and is equal to approximately 0.64 for these sands. Equation (40) can be useful in cases where one of the necessary light transmission images for the determination of liquid saturation is unavailable ( $I_s$ ,  $I_d$ , or  $I_{res}$ ).

**5.2. Closed-Form Solution for Saturations Above Residual**

[36] Best fits of both the Brooks and Corey (shaded lines; equation (23)) and van Genuchten (solid lines; equation (29)) models are shown in Figure 5 to the primary drainage  $\Omega$ - $h$  data for the four grades of Accusand. The two empirical approximations are nearly indistinguishable for the coarser sand grades (12/20 and 20/30), except in the vicinity of the air-entry pressure head. The van Genuchten model fits the data slightly better for the finer sands in the dry end. Table 3 lists the optimized parameters for both models. The incomplete beta function  $I'_u(w', z')$  was evaluated with Microsoft Excel 2000 using the function BETADIST( $u'$ ,  $w'$ ,  $z'$ , 0, 1). The closed-form solutions all had  $R^2$  values very close to 1, with variations from unity apparent after the fourth decimal place.

**5.3. Saturations Below Residual**

[37] A comparison of the predicted versus measured water removed from the chamber is shown in Figure 6. The correlation is perfect within the first two decimal



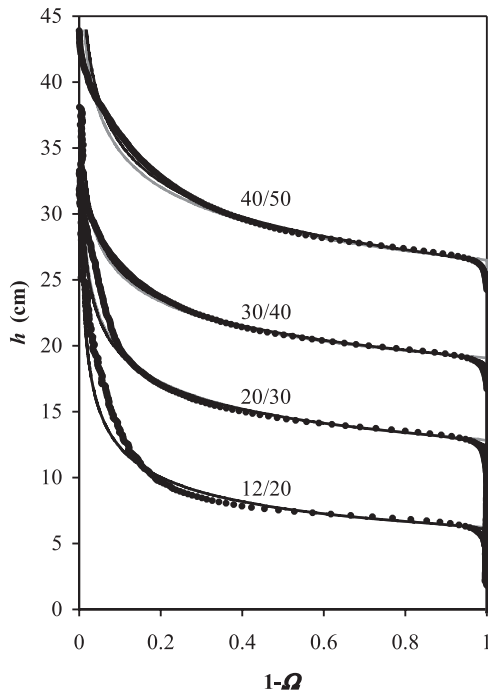


**Figure 5.** Fit of the Brooks and Corey and van Genuchten type approximations to  $\Omega$ - $h$  data for the four grades of Accusand. The van Genuchten type functions (equation (24)) are shown as solid lines, and the Brooks and Corey type functions are shown as shaded lines (equation (21)).

places,  $R^2 = 1.00$ , if the first three data points are disregarded. These three points were obtained before the installation of a convective heater and drop tube (Figure 1). These items prevented the condensation of water in the tubing between the chamber and desiccator, and the region of the chamber above the sand, resulting in water that was removed from the sand in the chamber not being measured in the desiccator.

[38] Pumping dry air upward through the chamber caused the sand pack to dry from the sides and top edges toward the center. Figure 7 shows the saturation distribution in the chamber at an intermediate stage of the experiment. This drying pattern was caused by the diversion of gas flow around the relatively wet sand near the lower manifold to the outer edges, where a preferential path was established along the O-ring seals. The sand near the outer edges dried first, establishing a self-propagating high-conductivity gas conduit.

[39] Since a mass balance was performed over the whole sand-filled domain the pattern of drying was not of primary

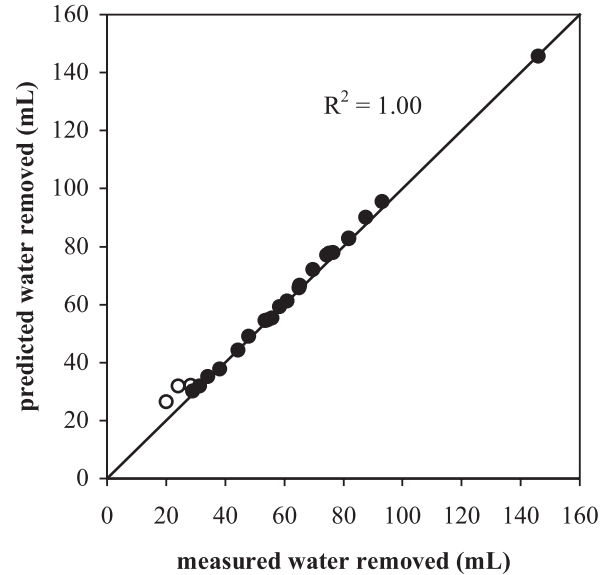


**Figure 6.** Comparison of predicted water removed versus measured water removed from the entire chamber. The chamber was packed with 40/50 sand. The first three data points (shown in open circles) were obtained at a time when water condensate existed in the tubing and on the glass above the sand surface, and were disregarded in the  $R^2$  value.

concern in this experiment. The goal was to achieve a situation where a significant portion of the media was between residual saturation and air-dry conditions. The resulting drying pattern was fortuitous from this standpoint in that the drying rind covered much more area than the anticipated horizontal, upward advancing, drying front. Figure 8 presents the water in the chamber that existed above and below residual saturation for each transmission image taken throughout the drying experiment. The amount of water present in the chamber below residual saturation increased and plateaued at about 14 mL, then dropped to zero, while the water above residual saturation continuously declined over the course of the experiment. Overall, about 147 mL of water were removed from the chamber intermittently over a 6-week period in a series of ten  $\sim$ 5-hour cycles, with the last cycle running overnight until dry.

## 6. Summary and Conclusions

[40] Quantification of liquid saturation and gas-liquid interfacial area is often essential in studies involving unsaturated porous media. In this work a relationship was developed to estimate the total available specific air-water interfacial area (at residual saturation) of a porous medium from the primary drainage pressure-saturation characteristic curve. The relationship was shown to accurately reproduce the results of a separate independent study, as opposed to other methods for the measurement of air-water interfacial area at residual saturation. Further research is needed to evaluate the effectiveness of this model throughout the full range of the primary drainage curve, as well on hysteretic loops.

**Table 3.** Parameters for Approximations of  $\Omega$ - $h$  Data

Sand	Brooks and Corey		van Genuchten		
	$h_d$	$\lambda'$	$\alpha$	$m'$	$n'$
12/20	6.2	3.4	0.160	0.0515	66
20/30	12.9	5.5	0.0775	0.0840	67
30/40	19.1	8.0	0.0523	0.0783	99
40/50	26.5	8.5	0.0377	0.0802	100

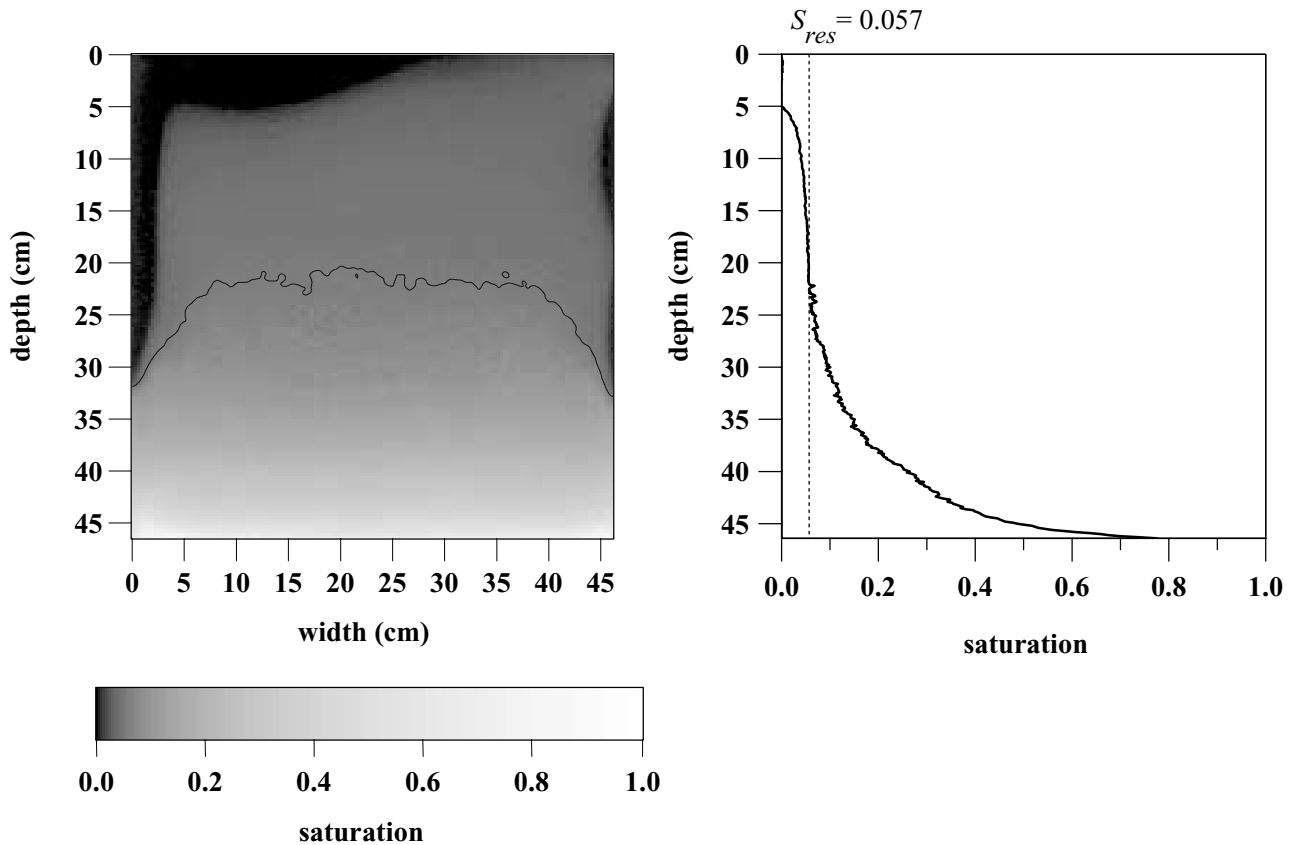


**Figure 7.** Saturation distribution at the end of the drying experiment with 40/50 sand. The left panel shows the saturation image plotted using a logarithmic gray scale palette. A contour line is shown at residual saturation ( $S_{res} = 0.057$ ); the pixels above the contour line were less than  $S_{res}$  and the pixels below the contour line were greater than  $S_{res}$ . The right panel shows a vertical transect for the column of pixels at 10 cm width.

[41] Past work has indicated that the fraction of gas-liquid interfacial surface area exposed at a given liquid saturation controls the relative degree of transmitted light. The accurate prediction of liquid saturation obtained with this method, throughout the full range of saturation, suggests a link between liquid saturation and gas-liquid interfacial area under the specific conditions considered. This link is based on surface area to volume ratio for the specific pore geometry, as illustrated in equation (6). The results of this work showed a linear correspondence between the log-scaled relative degree of light transmission and the inverse of grain size, under dry and residually saturated conditions. This is to be expected for geometrically similar media, such as those used in this study, provided light transmission is representative of the interfacial surface area.

[42] Two closed-form solutions were presented relating liquid saturation to light transmission above residual saturation. The previously published method requires numerical integration of the  $\Omega$ - $h$  characteristic curve to establish this relationship, followed by a subsequent fit with a fourth-order polynomial to obtain a continuous solution. The analytical solutions presented here utilized the commonly used functional forms presented by *Brooks and Corey* [1964] and *van Genuchten* [1980] to fit the  $\Omega$ - $h$  data, and produced results essentially identical to the numerical approach.

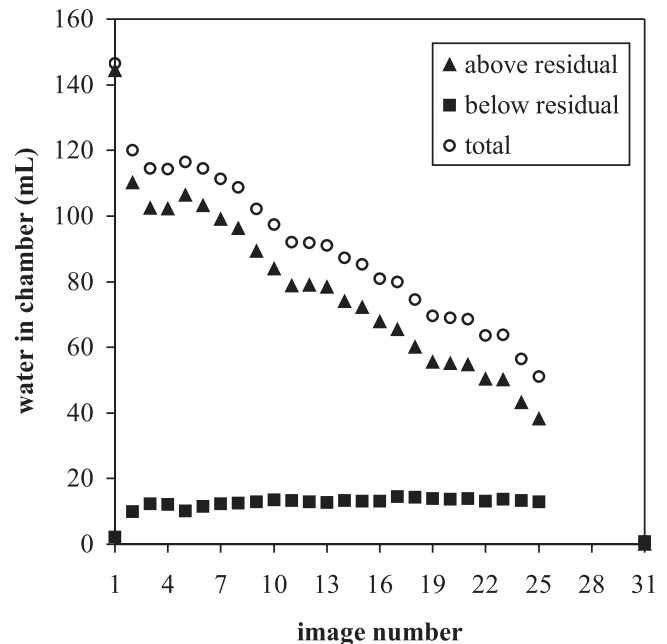


**Figure 8.** Comparison of water remaining in the chamber above and below residual saturation for each image obtained throughout the drying experiment with 40/50 sand.

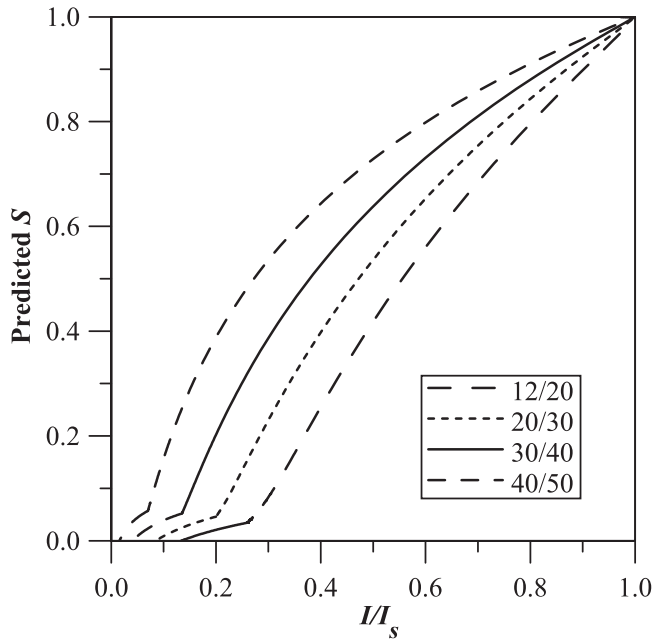


**Figure 9.** Relationship between absolute liquid saturation and the relative degree of light transmission. Note the discontinuity at residual saturation where the prediction of  $S$  switches from equation (20) above residual to equation (36) below residual.

[43] A physical model was developed and tested to quantify liquid saturation below residual from the relative degree of light transmission. Again, exposed interfacial area controls the process; however, in this case, the gas-liquid films give way to less transmissive gas-solid interfaces, resulting in a discontinuous relationship between light transmission and saturation between air-dry and fully saturated conditions. An accurate mass balance was achieved in an experiment where nearly 150 mL of water were evaporated from a sand-packed chamber, where most of the pack was initially near residual saturation. A separate model was used for locations that were above residual saturation. Figure 9 illustrates the discontinuous behavior of the relative degree of light transmission over the full range of saturation for the four grades of sand. The transition between the two light transmission processes is apparent at the point  $(I_{res}/I_s, S_{res})$ , which occurs around 5% saturation.

[44] In laboratory systems, light transmission holds great promise as a nondestructive, noninvasive, analytical tool to measure the full range of liquid saturation and gas-liquid interfacial area accurately and efficiently. This is of interest in a multitude of studies, such as the partitioning of solutes and microorganisms to interfacial surfaces, and vapor transport from residually saturated porous media.

[45] **Acknowledgments.** Funding for this project was provided by the National Science Foundation (grant 9630293) and the Department of Energy (grants DE-FG07-98ER14925 and DE-FG07-99ER62887). Special thanks to Rockie Yarwood for his help in the lab.

## References

- Abramowitz, M., and I. A. Stegun, *Handbook of Mathematical Functions*, Dover, Mineola, N. Y., 1965.
- Bear, J., *Dynamics of Fluids in Porous Media*, Dover, Mineola, N. Y., 1972.
- Bradford, S. A., and F. J. Leij, Estimating interfacial areas for multi-fluid soil systems, *J. Contam. Hydrol.*, 27, 83–105, 1997.
- Brooks, R. H., and A. T. Corey, Hydraulic properties of porous media, *Hydrol. Pap. 3*, Colo. State Univ., Fort Collins, 1964.
- Carter, D. L., M. M. Mortland, and W. D. Kemper, Specific surface, in *Methods of Soil Analysis: Part 1—Physical and Mineralogical Methods*, 2nd ed., edited by A. Klute, pp. 413–423, Am. Soc. of Agron., Madison, Wisc., 1986.
- Cary, J. W., Estimating the surface area of fluid phase interfaces in porous media, *J. Contam. Hydrol.*, 15, 243–248, 1994.
- Darnault, C. J. G., J. A. Throop, D. A. DiCarlo, A. Rimmer, T. S. Steenhuis, and J.-Y. Parlange, Visualization by light transmission of oil and water contents in transient two-phase flow fields, *J. Contam. Hydrol.*, 31, 337–348, 1998.
- Darnault, C. J. G., D. A. DiCarlo, T. W. J. Bauters, A. R. Jacobson, J. A. Throop, C. D. Montemagno, J.-Y. Parlange, and T. S. Steenhuis, Measurement of fluid contents by light transmission in transient three-phase oil-water-air systems in sand, *Water Resour. Res.*, 37, 1859–1868, 2001.
- DiCarlo, D. A., T. W. J. Bauters, C. J. G. Darnault, T. S. Steenhuis, and J.-Y. Parlange, Lateral expansion of preferential flow paths in sands, *Water Resour. Res.*, 35, 427–434, 1999.
- Frankenfield, J., and J. S. Selker, Fluid interfacial geometry at the pore scale and its effects on characteristic curves, in *Proceedings of the 14th Annual Hydrology Days*, pp. 111–122, Hydrol. Days Publ., Atherton, Calif., 1994.
- Gardner, W. H., Water content, in *Methods of Soil Analysis: Part 1—Physical and Mineralogical Methods*, 2nd ed., edited by A. Klute, pp. 528–541, Am. Soc. of Agron., Madison, Wisc., 1986.
- Gvrtzman, H., and P. V. Roberts, Pore-scale spatial analysis of two immiscible fluids in porous media, *Water Resour. Res.*, 27, 1165–1176, 1991.
- Karkare, M. V., and T. Fort, Determination of the air-water interfacial area in wet “unsaturated” porous media, *Langmuir*, 12, 2041–2044, 1996.
- Kechavarzi, C., K. Soga, and P. Wiart, Multispectral image analysis method to determine dynamic fluid saturation distribution in two-dimensional three-fluid phase flow laboratory experiments, *J. Contam. Hydrol.*, 46, 265–293, 2000.
- Kelly, S. F., and J. S. Selker, Osmotically driven water vapor transport in unsaturated soils, *Soil Sci. Soc. Am. J.*, 65, 1634–1641, 2001.
- Kim, H., P. S. C. Rao, and M. D. Annable, Determination of effective air-water interfacial area in partially saturated porous media using surfactant adsorption, *Water Resour. Res.*, 33, 2705–2711, 1997.
- Leverett, M. C., Capillary behavior in porous solids, *Trans. Am. Inst. Min. Metall. Pet. Eng.*, 142, 152–169, 1941.
- Liu, Y., B. R. Bierck, J. S. Selker, T. S. Steenhuis, and J.-Y. Parlange, High intensity X-ray and tensiometer measurements in rapidly changing preferential flow fields, *Soil Sci. Soc. Am. J.*, 57, 1188–1192, 1993.
- Miller, C. T., M. M. Poirier-McNeill, and A. S. Mayer, Dissolution of trapped nonaqueous phase liquids: Mass transfer characteristics, *Water Resour. Res.*, 26, 2783–2796, 1990.
- Mortensen, A. P., R. J. Glass, K. Hollenbeck, and K. H. Jensen, Visualization of microscale phase displacement processes in retention and outflow experiments: Nonuniqueness of unsaturated flow properties, *Water Resour. Res.*, 37, 1627–1640, 2001.
- Niemit, M. R., and J. S. Selker, A new method for quantification of liquid saturation in 2-D translucent porous media systems using light transmission, *Adv. Water Res.*, 24, 651–666, 2001.
- Oostrom, M., C. Hofstee, J. H. Dane, and R. J. Lenhard, Single-source gamma radiation procedures for improved calibration measurements in porous media, *Soil Sci.*, 163, 646–656, 1998.
- Reeves, P. C., and M. A. Celia, A functional relationship between capillary pressure, saturation, and interfacial area as revealed by a pore-scale network model, *Water Resour. Res.*, 32, 2345–2358, 1996.
- Rimmer, A., D. A. DiCarlo, T. S. Steenhuis, B. Bierck, D. Dunford, and J.-Y. Parlange, Rapid fluid content measurement method for fingered flow in an oil-water-sand system using synchrotron X-rays, *J. Contam. Hydrol.*, 31, 315–334, 1998.
- Saripalli, K. P., H. Kim, P. S. C. Rao, and M. D. Annable, Measurement of specific fluid-fluid interfacial areas of immiscible fluids in porous media, *Environ. Sci. Technol.*, 31, 932–936, 1997.
- Schaefer, C. E., D. A. DiCarlo, and M. J. Blunt, Experimental measurement of air-water interfacial area during gravity drainage and secondary imbibition in porous media, *Water Resour. Res.*, 36, 885–890, 2000.
- Schäfer, A., P. Ustohal, H. Harms, F. Stauffer, T. Dracos, and A. J. B. Zehnder, Transport of bacteria in unsaturated porous media, *J. Contam. Hydrol.*, 33, 149–169, 1998.
- Schroth, M. H., S. J. Ahern, J. S. Selker, and J. D. Istok, Characterization of

- Miller-similar silica sands for laboratory hydrologic studies, *Soil Sci. Soc. Am. J.*, *60*, 1331–1339, 1996.
- Skopp, J., Oxygen uptake and transport in soils: Analysis of the air-water interfacial area, *Soil Sci. Soc. Am. J.*, *49*, 1327–1331, 1985.
- Tidwell, V. C., and R. J. Glass, X ray and visible light transmission for laboratory measurement of two-dimensional saturation fields in thin-slab systems, *Water Resour. Res.*, *30*, 2873–2882, 1994.
- van Genuchten, M. T., A closed form equation for predicting the hydraulic conductivity of unsaturated soils, *Soil Sci. Soc. Am. J.*, *44*, 892–898, 1980.
- Weisbrod, N., T. McGinnis, M. R. Niemet, and J. S. Selker, Infiltration mechanisms of highly saline solutions and possible implications for the Hanford Site, *Eos Trans. AGU*, *81*(48), Fall Meet. Suppl., Abstract H61A-04, 2000.
- Weisbrod, N., M. R. Niemet, and J. S. Selker, Imbibition of saline solutions into dry and pretreated porous media, *Adv. Water Resour.*, in press, 2002.
- 
- M. R. Niemet, CH2M Hill, 2300 N.W. Walnut Boulevard, Corvallis, OR 97330, USA. (mniemet@ch2m.com)
- M. L. Rockhold, Pacific Northwest National Laboratory, Box 999, Richland, WA 99352, USA.
- J. S. Selker, Department of Bioengineering, Oregon State University, Corvallis, OR 97331, USA.
- N. Weisbrod, Department of Environmental Hydrology and Microbiology, Ben-Gurion University of the Negev, Sde-Boqer 84933, Israel.